EUROPEAN ORGANIZATION FOR NUCLEAR RESEARCH
European Laboratory for Particle Physics

The Alice Silicon Drift Detector System

Authors:

D. Nouais, S. Beolè, M. Bondila, V. Bonvicini, P. Cerello, E. Crescio,
P. Giubellino, M. Idzik, A. Kolozhvari, S. Kouchpil, E. Lopez Torres,
M.I. Martinez, G. Mazza, S. Piano, C. Piemonte, A. Rashevsky, L. Riccati,
A. Rivetti, F. Tosello, W.H. Trzaska, A. Vacchi, R. Wheadon
for the ALICE collaboration

The Alice Silicon Drift Detector System

D. Nouais [a,1], S. Beolè [a], M. Bondila [b,2], V. Bonvicini [c],
P. Cerello [a], E. Crescio [a], P. Giubellino [a], M. Idzik [a],
A. Kolozhvari [a,b], S. Kouchpil [d], E. Lopez Torres [a],
M.I. Martinez [a,e], G. Mazza [a], S. Piano [c], C. Piemonte [c],
A. Rashevsky [c], L. Riccati [a], A. Rivetti [a], F. Tosello [a],
W.H.Trzaska [b], A. Vacchi [c], R. Wheadon [a],
for the ALICE collaboration.

[a]*INFN Sezione di Torino, Italy*

[b]*Jyväskylä University, Finland*

[c]*INFN Sezione di Trieste, Italy*

[d]*Řež, Czeck Republic*

[e]*CINVESTAV Mexico City, Mexico*

Abstract

The project of the two Silicon Drift Detector layers of the ALICE Inner Tracking System is reviewed. Recent results obtained from beam tests are presented.

1 Introduction

The central detector of ALICE [1,2] will consist of an Inner Tracking System (ITS) [3,4] whose basic functions are the secondary vertex reconstruction of hyperon and charm decays, the particle identification and the tracking of low-momentum particles, and the improvement of the overall momentum resolution. The system, which covers the polar angular range $90 \pm 45\,\mathrm{deg}$ over the full azimuth, is embedded in a large solenoidal magnet generating a field between $0.2\,\mathrm{T}$ e $0.5\,\mathrm{T}$. Because of the high particle density, the innermost four layers need to be truly two-dimensional devices. To give the inner tracking system a stand-alone particle identification capability, a minimum of four layers

---

[1] Corresponding author. E-mail: nouais@to.infn.it
[2] also at Institute of Space Sciences, Bucharest

need an analogue readout with a wide enough dynamic range to provide un-saturated dE/dx measurements down to the minimum momentum for which the tracks have a reasonable ($> 20\%$) reconstruction probability. To achieve this performance, the ITS will consist of six barrels of high-resolution silicon tracking detectors:

- two layers of silicon pixel detectors (SPD's) with digital readout,
- two layers of silicon drift detectors (SDD's)with analogue readout,
- two layers of double-sided silicon micro-strip detectors (SSD's) with ana-logue readout.

Silicon drift detectors have been chosen to equip the third and the fourth layers of the ITS, due to their characteristics: very high-resolution two dimensional sensors suitable for high track-density experiments with low rate, because of their relatively slow readout (a few microseconds). In an SDD, the electrons released during the passage of a particle drift under the effect of an applied electric field along a direction parallel to the surface of the wafer towards an array of collecting anodes. The drift velocity is proportional to the electric field E and to the electron mobility μ_e: $v = \mu_e E$. In this way, the distance of the crossing point from the anodes is determined by the measurement of the drift time. The second coordinate is obtained from the centroid of the charge distribution across the anodes. As a consequence of this principle the number of front-end channels necessary to read out large area detectors is very small compared to other detectors with comparable spatial resolution. The reduced number of electronic channels allows the front-end to provide the energy loss measurement without increasing too much the power budget.

In Section 2 the ALICE SDD system will be described, including the detector design and an overview of the readout architecture. In Section 3 beam test results for the spatial resolution of a final detector prototype will be discussed.

2 The Silicon Drift Detector system

The SDD's have to provide a spatial precision of about 30 μm, and a two-track separation down to $O(600)$ μm. In addition the charge resolution should allow a dE/dx resolution dominated by Landau fluctuations.

2.1 The detector

The ALICE SDD final prototypes[5] were produced by Canberra Semiconduc-tor on 300 μm thick 5" Neutron Transmutation Doped (NTD) wafers with a

resistivity of 3 kΩcm (Fig. 1). Their active area is $7.02 \times 7.53 \, \text{cm}^2$ and the ratio to the total detector area ($7.25 \times 8.76 \, \text{cm}^2$) is 0.85. The active area is split into two adjacent 35 mm long drift regions, each equipped with 256 collecting anodes ($294 \, \mu\text{m}$ pitch) and with integrated voltage dividers for the drift and the guard regions. A careful design of the cathode strips prevents any punch-through which would deteriorate the voltage divider linearity. Since the drift velocity is very sensitive to the detector temperature variation ($v \propto T^{-2.4}$), the monitoring of this quantity is performed by means of three rows of 33 implanted point-like MOS charge injectors[6,7].

2.2 The SDD barrel

The SDD's are mounted on linear supports, called ladders, manufactured using Carbon-Fibre Reinforced Plastic (CFRP) to minimize the material budget. The inner SDD layer is composed of 14 ladders, each holding six detectors. It has on average a radius of 14.9 cm and a 595 mm length. The outer layer is made of 22 ladders supporting eight detectors each. It has a radius of 23.8 cm and a 670 mm length. 260 SDD's are needed to cover the two layers. In every ladder the detectors are mounted at different distances from the support structure and the ladders are assembled at different radii from the beam axis in order to allow small overlaps of the detector active areas. This is necessary to ensure the full coverage for all possible vertex positions and all tracks within the acceptance. The SDD ladders are assembled onto a CFRP mechanical support made up of two end-cap cones connected by a thin cylinder. The orientation of the SDD's anodes along the ladders, chosen to make the assembly procedure simpler, makes the drift velocity orthogonal to the beam axis and therefore to the magnetic field. The Lorenz force acts perpendicularly to the detector plane and is compensated by the focusing electric drift field.

2.3 The SDD readout

The readout and data transmission of the whole SDD barrel is subdivided in half ladders. The total readout time of the SDD should be lower than 1 ms. A block diagram of the readout of a half ladder of the third layer is shown in Fig. 2. A 256–channel front-end hybrid circuit, connected to each half detector, performs the preamplification and the analogue to digital conversion of the SDD signal, and transmit the data to the end ladder. The power consumption of the front end electronics has to be as low as possible due to the high sensitivity of the detector to temperature variations and to the limited material for cooling that can be located on the ladder structure. The SDD front-end electronics is based on two 64 channel ASICs named PASCAL[8]

and AMBRA[9]. Four pairs of chips per hybrid are needed in order to read out a half SDD.

PASCAL provides both the preamplification and the digitization. It has a dynamic range of 32 fC which is necessary to meet the requirements for low momentum particle identification. To achieve the expected spatial resolution of the detector, the preamplifier has been designed to have an equivalent noise charge of $250\,e^-$ and the A/D converter to have 10-bit precision. The clock frequency of LHC, 40 MHz, has been chosen as the sampling frequency for the SDD signal. The preamplifier peaking time (40 ns) was chosen as short as possible so as to have a satisfactory double track resolution, within the limit of ensuring a good sampling of the signal for all drift times. Since the power consumption of an A/D converter operated at 40 Msample/s would be unacceptable, PASCAL contains an intermediate, 256 channel, analogue ring memory for each channel which samples the output of the preamplifier every 25 ns. When a trigger is received the contents of the analogue memories are frozen and then read out by the ADC's (one ADC per two channels) with a conversion rate of 2 Msample/s, for a total readout time of about $250\,\mu$s.

The second ASIC, AMBRA, is a multi-event buffer which is necessary in order to reduce the needed bandwidth for the data transmission without increasing the average detector dead time. The data coming from PASCAL are written in one of the four digital buffers of AMBRA which derandomizes the events. AMBRA also implements a 10-bit to 8-bit data compression using a scheme chosen to keep the percentage quantization error almost constant.

The data are transferred at 40 MHz from the four AMBRA's of each half-detector to the end–ladder modules. A third ASIC (CARLOS) performs the zero-suppression and the compression of the data [10] before their transmission to the DAQ system. CARLOS also takes care of the interface with the trigger system via the TTCrx chip.

The three ASICs, PASCAL, AMBRA and CARLOS, are implemented in a commercial $0.25\,\mu$m CMOS technology, using radiation-tolerant layout techniques developed by the CERN RD49 collaboration[11].

2.4   Assembly of the SDD modules

The main building element of the SDD subsystem (module) is based on a single drift detector connected to two hybrid circuits. The front-end hybrid carries four AMBRA–PASCAL pairs to equip the 256 anodes of a half–detector. Each pair PASCAL–AMBRA is first assembled with an aluminum–Upilex microcable [12] which is then TAB bonded to the hybrid circuit layer and to the detector anodes. Finally, each hybrid circuit is glued with a thermo-conductive

compound on a 100 micron carbon fibre *heat bridge* substrate which is then clipped to the cooling tubes mounted on the sides of the ladder frames.

The interface cards between the modules and the cables to the ITS patch panels carrying signals and power are placed in the end-ladder region. One low voltage (LV) card per hybrid provide individual power supply regulation, signal interfacing to the data reduction electronics and slow control circuitry. The signal and power connection between the LV cards and the hybrids is provided by Aluminum–Upilex low thickness microcables (20 μm Upilex + 30 μm Al). One high voltage (HV) card per SDD carries the filter capacitors and DC-blocking capacitors for the injector pulses. Development of microcables capable of carrying the high voltage (up to 2.4 kV) from the HV cards to the SDD is in progress.

3   Beam test results

3.1   Experimental details

Due to the complexity of the PASCAL ASIC, the first-full chain prototype ha only recently been produced. Previous SDD tests were, instead, performed with the OLA[13] preamplifier. OLA is a 32-channels, low-noise, bipolar VLSI circuit specifically designed for SDD's. Each OLA channel features a charge-sensitive preamplifier, a semi-Gaussian shaping amplifier and a symmetrical line driver. The peaking time is 55 ns for a δ-like input signal and the Equivalent Noise Charge (ENC) was measured to be $\sim 230\,e^-$ at zero detector capacitance. The preamplifier was followed by a voltage amplifier driving a 30 m long twisted-pair cable connected to a flash-ADC system[14] which sampled the signal at 40 MHz. The ADC system had 8-bit resolution and a non-linear transfer function expanding the dynamic range to 10 bits.

Since 1997, several tests have been performed using CERN-PS and -SpS high momentum (approximately minimum ionizing) particle beams. The typical experimental setup was built in the following way: one or more (up to three) SDD prototypes were placed on the beam line within a microstrip telescope used to measure the impact point of the particle tracks on the SDD planes. The telescope was made up of five pairs of single sided silicon strip detectors alternating horizontal and vertical planes. Each plane had an area of 20 * 19.2 mm and a strip pitch of 50 μm. Two pairs (upstream and downstream) of 2 cm–wide crossed scintillator were used to select only the particles passing through the telescope. Since the area covered by the microstrip detectors was smaller than the SDD sensitive area, the SDD's were mounted on a mobile support whose position was remotely controlled and measured with a precision

of about $30 \, \mu$m.

3.2 Dopant inhomogeneity and spatial resolution

Even if the ALICE SDD's are produced on NTD wafers, which are expected to have a particularly uniform dopant concentration, characteristic effects of inhomogeneity, large enough to deteriorate significantly the spatial resolution of the detectors, have already been observed[15]. Inhomogeneity of the dopant concentration alters the uniformity of the drift field superimposing a local parasitic field on the ideally constant one in the middle plane of the detector. The component of the parasitic field parallel to the drift direction locally change the drift velocity and so causes systematic errors in the measurement of the coordinate along the drift axis. The component of the parasitic field perpendicular to the drift direction induces deviations of the electron trajectories from the ideal linear path leading to systematic errors on the anodic coordinate. During a beam test performed on an ALICE SDD prototype of the final design, half a detector ($7.5 \times 3.5 \, \text{cm}^2$) was exposed to the beam, in order to evaluate its performance. The local systematic deviations can be evaluated by calculating within small areas the mean value of the residuals between the cluster centroid with respect to the impact point of the particle as measured by the microstrip telescope. Fig. 3 shows in gray scale the systematic deviations ΔX of the anodic coordinate (top) and ΔY along the drift coordinate (middle) assuming a constant drift velocity calculated for all the active area of half an SDD. The bottom plot shows as an example the systematic deviations calculated for both axes at $X = 20 \, \text{mm}$ as a function of the drift distance. Deviation of a few tens of μm in average and with maximum values up to $400 \, \mu$m are observed and must be corrected in order to reach the spatial resolution goal of about $30 \, \mu$m. The circular structures centered on the middle of the wafer, clearly observed in this plot, can be attributed to the characteristic radial dependence of the dopant concentration fluctuations. In addition to these source of electrostatic field, vertical structures are also seen. They are produced by anomalous electronics channel with unstable gain and/or long shaping time. The horizontal step in the middle of the second plot is caused by a short circuit between two cathodes which locally reduce the drift field. Fig. 4 shows the resolution along the anode and the drift-time directions obtained after the correction of these systematic deviations. The slight increase, from $30 \, \mu$m to $35 \, \mu$m, of the resolution along the drift direction can be attributed to the charge diffusion, which make the size of the charge cluster wider at larger drift times reducing in the same time the signal amplitude. The resolution along the anode direction has values better than $30 \, \mu$m over more than 80% of the whole drift path, with the best value reach $15 \, \mu$m at $15 \, \text{mm}$ from the anodes. The deterioration of the resolution at small drift distance is due to the small size of the electron cloud collected on the anodes. When the charge is collected

6

by two anodes, a correction can be applied to the anode charge distribution centroid in order to better determine the position of the crossing point of the particle[16]. The global improvement on the anodic resolution can be seen on the black circle curve.

4 Conclusions

In spite of the relevant effects of the dopant inhomogeneity of the wafers on which the SDD's are build, it has been demonstrated that the deviations can be measured and corrected, leading to a good resolution of the detector along both the anodic and the drift directions. Since it would be difficult to measure the deviation maps of all the 260 SDD's with a minimum ionizing particle beam, the possibility of a laser measurement is under study.

The analysis of the first beam tests using a single pair of the prototype versions of PASCAL and AMBRA to read out part of an ALICE SDD is now under way. Preliminary results indicate that the signal-to-noise performance, after correction for some systematic effects, is at least as good as that obtained with OLA.

References

[1] N. Antoniou *et al.*, CERN/LHCC/93–16 (1993).

[2] ALICE Collaboration, CERN/LHCC, 95/71

[3] ALICE Collaboration, CERN/LHCC, 99/12

[4] F. Tosello *et al.*, Nucl. Instr. and Meth. A473 (2001) 210-218.

[5] A. Rashevsky *et al.*, Nucl. Instr. and Meth. A 461 (2001) 133-138

[6] V. Bonvicini *et al.*, Il Nuovo Cim. A112 (1999) 137.

[7] V. Bonvicini *et al.*, Nucl. Instr. and Meth. A439 (2000) 476.

[8] A. Rivetti *et al.*, CERN-LHCC-2000-041

[9] G. Mazza *et al.*, CERN-LHCC-2001-034

[10] A. Werbrouck *et al.*, Nucl. Instr. and Meth. A471 (2001) 281-284.

[11] M. Campbell *et at.*, Nucl. Instr. and Meth. A473 (2001) 140-145

[12] A.P. De Haas *et al.*, CERN-LHCC-99-033

[13] W. Dabrowski *et al.*, Nucl. Phys. B 44 (1995) 637

[14] F. Balestra *et al.*, Nucl. Instr. and Meth. A323 (1992) 523.

[15] D. Nouais *et al.*, Nucl. Instr. and Meth. A 461 (2001) 133-138

[16] E. Crescio *et al.*, CERN-ALICE-PUB-2000-029, ALICE-INT-2001-09
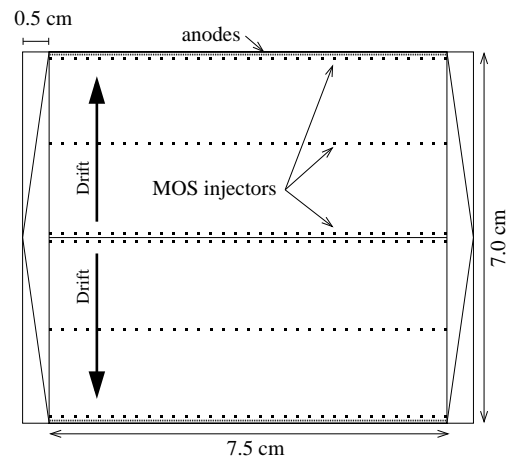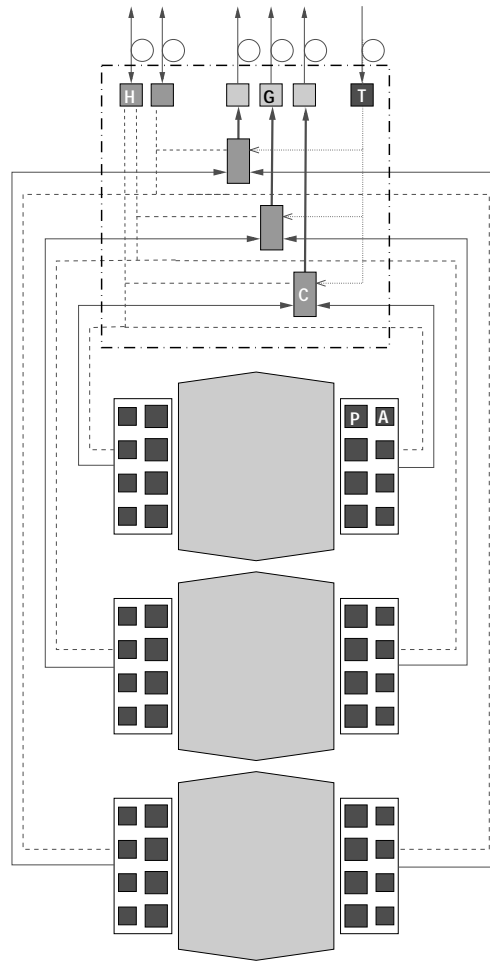
Fig. 1. Sketch of the final ALICE SDD prototype

Fig. 2. Readout block diagram of a half ladder of the third layer. (P: PASCAL (Preamplifier, Analogue Storage and Conversion from Analogue to digitaL), A: AMBRA (A Multievent Buffer Readout Architecture), C: CARLOS (Compression And Run Length encOding Subsystem), T: TTCrx (Timing, Trigger and Control receiver), G: GOL (Gigabit Optical Link), H: HAL (Hardware Abstraction Layer)
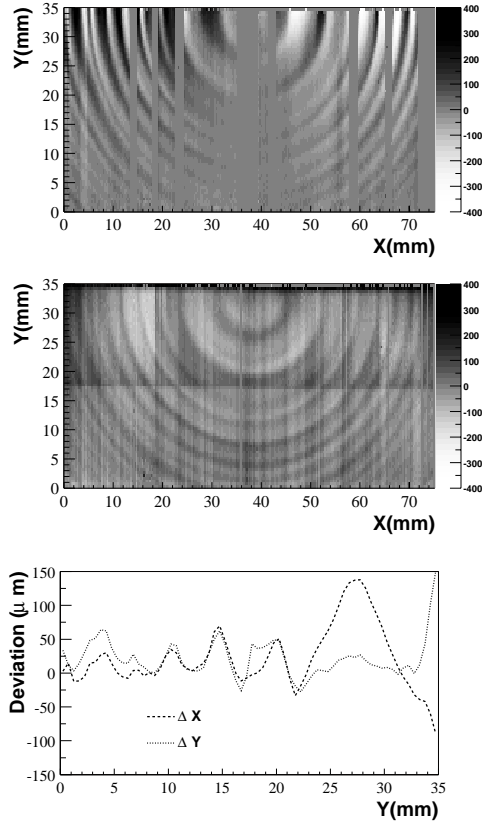
Fig. 3. Systematic deviations (gray scale in μm) of the anodic $\Delta X(X,Y)$ (top) and drift coordinates $\Delta Y(X,Y)$ (middle) of the electron cloud centroid with respect to the reference position of the crossing point of the particle coordinate, as a function of the anodic coordinate X, and the drift distance Y. Bottom plot: $\Delta X(X,Y)$ and $\Delta Y(X,Y)$ as a function of the drift distance for $x = 20\,\mathrm{mm}$.
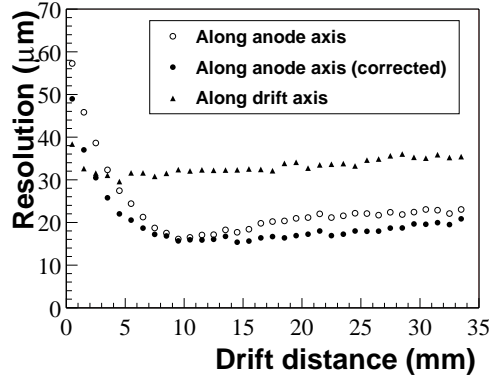

Fig. 4. Spatial resolution of the ALICE SDD along the drift-time axis and anode axis as function of the drift distance.